Erosion Corrosion Behavior of Aluminum Electrode in Simulated HVDC Water Cooling at 50 °C

Jiayang Li[1], Liangshou Hao[1], Feng Zheng[1], Xiaoping Chen[1], Shengping Wang[2,],Youping Fan[3,*]*

[1] Tianshengqiao Bureau, Extra High Voltage Power Transmission Company, China Southern Power Grid (CSG), Xingyi 562400, China
[2] Faculty of Material Science and Chemistry, China University of Geosciences, Wuhan 430074, China
[3] School of Electrical Engineering and Automation, Wuhan University, Wuhan 430072, China
*E-mail: spwang@cug.edu.cn, ypfan@whu.edu.cn

The inner wall of aluminum radiators in a high voltage direct current (HVDC) thyristor valve cooling systems are corroded under a continuous erosion of water coolant at ~50 °C, and the dissolved aluminum ions precipitate again on the surface of the platinum grading electrode; thus, HVDC transmission is adversely affected. To clarify the corrosion characteristics of aluminum in HVDC, the erosion corrosion behaviors of aluminum in 50 °C deionized water under various water flow velocities are studied. With increasing water flow velocities, the corrosion current of aluminum gradually increases, the corrosion potential gradually decreases, the charge transfer impedance gradually decreases, and the corrosion of aluminum tends to become serious. Aluminum under a water flow velocity of 3 m s^{-1}, has the most negative corrosion potential (0.864 V), the maximum corrosion current (6.515×10^{-7} A cm^{-2}), the minimum charge transfer impedance (1.751×10^{-5} Ω), and the most serious erosion corrosion. In contrast, aluminum surfaces in unmoving water can form a passivating film to protect the interior. However, forced convection occurs when the water flow velocity reaches a certain value; the aluminum surfaces will undergo stress due to the impact of the flowing water, which destroys the passivation films and promotes the formation of forms an Al(OH)$_3$ corrosion product on the aluminum surface. The conclusion of this study will be helpful for the optimization of the technology and parameters in HVDC thyristor valve cooling systems.

1. INTRODUCTION

High voltage direct current (HVDC) transmission has become the preferred resource allocation and long-distance power transportation method because of its narrow transmission corridor, high transmission efficiency, and low power consumption [1, 2]. The inner wall of the aluminum radiator in

the HVDC thyristor valve cooling water system is corroded under the continuous erosion of deionized cooling water at ~50 °C. Its ionic conductivity is ~0.15 µS cm^{-1} [3], and the dissolved aluminum ions precipitate again on the surface of a platinum grading electrode; thus, HVDC transmissions are adversely affected [4, 5]. The basic reason for the scaling on the platinum grading electrode scaling is the corrosion of the aluminum radiator [6, 7]. Inhibiting the corrosion of the inner wall of the aluminum radiator is a key to solving the scaling of the platinum grading electrode. The corrosion behaviors of aluminum immersed in unmoving deionized water, ammonia [8], carbon dioxide [9] and sodium bicarbonate [10] have been studied previously. However, in practical work, cooling water in the HVDC cooling system is in constant circulating flow. The inner walls of the aluminum radiator are corroded when it comes into contact with the cooling water, and the aluminum is constantly dissolved in the water. Then, the aluminum ions move to the surface of the platinum grading electrode, and aluminum sediments are formed under the electric field. To clarify the corrosion law of aluminum in this particular environment, it is necessary to study the corrosion behavior of aluminum in flowing water.

The aluminum in flowing water undergoes a combination of erosion and corrosion [11]. The combined effects make the corrosion of aluminum more serious, and the corrosion degree far exceeds the result of corrosion on its own. The corrosion of aluminum by fluid erosion includes two factors. Increasing the oxygen supply accelerates the repassivation of passivated metals and accelerates the electrochemical corrosion of nonpassivated metals [12]. Mechanical action would destroy the passivation film on the surface. In addition, fluid erosion on the aluminum surface would make the surface uneven, and the corrosion would accelerate [13].

In general, the mechanical wear of metals by a fluid play a major role in erosion corrosion [14], and electrochemical corrosion also plays an important role [15]. Electrochemical corrosion is mainly related to the composition, concentration and type of solution, and the dissolved oxygen, pH [16] and temperature [17]. Corrosion is related to the repair and destruction of the passivation film on the metal surface, and electrochemical corrosion is also related to the flow rate of the electrolyte [18].

When the inner wall of the aluminum radiator in the HVDC cooling system is exposed to deionized water with high water flow velocities, erosion has a great impact on aluminum corrosion. In this paper, deionized water in the pipeline is used to erode the aluminum surface with water flow velocities by means of pipe flow experiments. The erosion corrosion law of aluminum at various water flow velocities is studied, and a theoretical basis for better corrosion protection of aluminum in a flow system is provided.

2. EXPERIMENTAL SECTION

2.1. Erosion corrosion experiment

The experimental device used for the erosion corrosion tests is shown in Fig. 1.
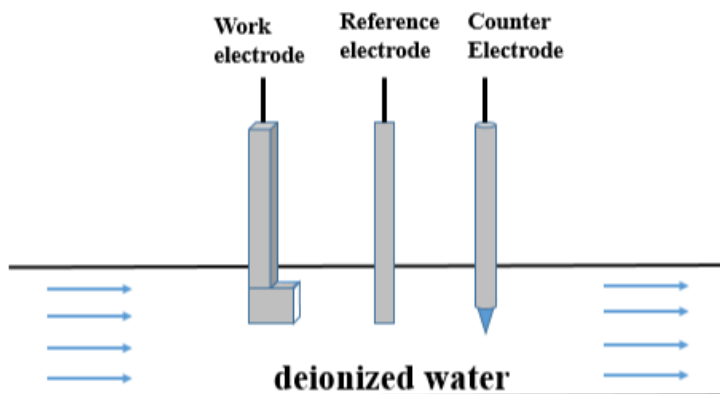
Figure 1. Diagram of the experimental device used for the erosion corrosion tests.

A pipe flow experimental method was used for testing. The aluminum working electrode, the auxiliary electrode and the reference electrode were fixed in a Teflon pipe (its diameter was 10 cm). A rotameter was used to control the flow rate of the deionized water in the pipe, and the water flow rates were 1, 1.5, 2, 2.5 and 3 m s^{-1}.

2.2. Electrochemical system

The aluminum work electrodes were cut from an aluminum radiator, which was composed of Si (0.57 wt%), Fe (0.63 wt%), Cu (0.14 wt%), Mn (1.27 wt%), Zn (0.09 wt%), Li (0.03 wt%) and Al (97.31 wt%) [19]. A 1 cm^2 work surface of the electrode was retained, and the rest was coated with epoxy resin. Before testing, the working electrodes were polished with diamond paper and nanoalumina powder and cleaned with deionized water and absolute ethanol.

A platinum black electrode was used as the counter electrode, and the reference electrode was a saturated calomel electrode (SCE); its potential at 50 °C was 0.228 V (relative to the standard hydrogen electrode (SHE)). The electrolyte was deionized water with a conductivity of ~0.15 uS cm^{-1}, and the water temperature was controlled at 48-52 °C. The above are the same as the working conditions of an HVDC water cooling system.

2.3. Electrochemical test

The potentidynamic polarization curves and electrochemical impedance spectroscopy (EIS) spectra were obtained using a CHI660D electrochemical workstation. The potentidynamic polarization curves were tested at the open circuit potential, and the potential scan rate was 1 mV s^{-1}. The potential range was 0.8 V (ranging from 0.4 V lower than the stable potential to 0.4 V higher than the stable potential). The corrosion potentials and corrosion current densities of the aluminum electrodes were obtained from the potentidynamic polarization curves. The corrosion characteristics of the aluminum electrodes were determined from the EIS analysis results that were tested at the open circuit potential. The frequency range was from 1 Hz to 10^5 Hz with an amplitude of 5 mV.

The working electrodes were eroded for 1, 3, 5, 7 and 9 h, and then the potentidynamic polarization curve test and the EIS test were conducted. The stable potential in each electrochemical test was recorded.

2.4. Characterization

The morphologies and compositions of the covering and corrosion products formed on the aluminum electrode surface, after being subjected to accelerated corrosion by potentiostatic anodic oxidation for 0.5 h, were determined for all samples by using scanning electron microscopy (SEM), energy dispersive spectrometry (EDS), Fourier transform infrared (FTIR) spectroscopy and X-ray diffraction (XRD). The constant potential of anodic oxidation was -0.5 V vs. Pt [20, 21]. Platinum was used as the cathode, a 1 cm×1 cm aluminum foil after polishing and washing was used as the anode, and deionized water was used as the electrolyte at 48-52 °C.

The compositions of the corrosion products were determined using a D8-Focus X-ray powder diffraction instrument with a Cu target. The scanning angle range was from 5 to 80 degrees, and the scan rate was $8°$ min^{-1}. The chemical bonds of the corrosion products were characterized using a Nicolet 6700 Fourier transform infrared spectrometer. SEM was performed using an SU8010 ultrahigh-resolution field emission scanning electron microscope equipped with high-performance X-ray energy dispersive spectroscopy.

3. RESULTS AND DISCUSSION

3.1. Potentidynamic polarization curves

The potentidynamic polarization curves of aluminum electrodes are shown in Fig. 2. The corrosion potential of aluminum electrodes negatively shifted with increasing water flow velocity. This indicated that the aluminum corrosion gradually increased. Moreover, with increasing erosion time, the corrosion potentials of the aluminum electrodes under various water flow velocities were relatively stable and hardly changed.
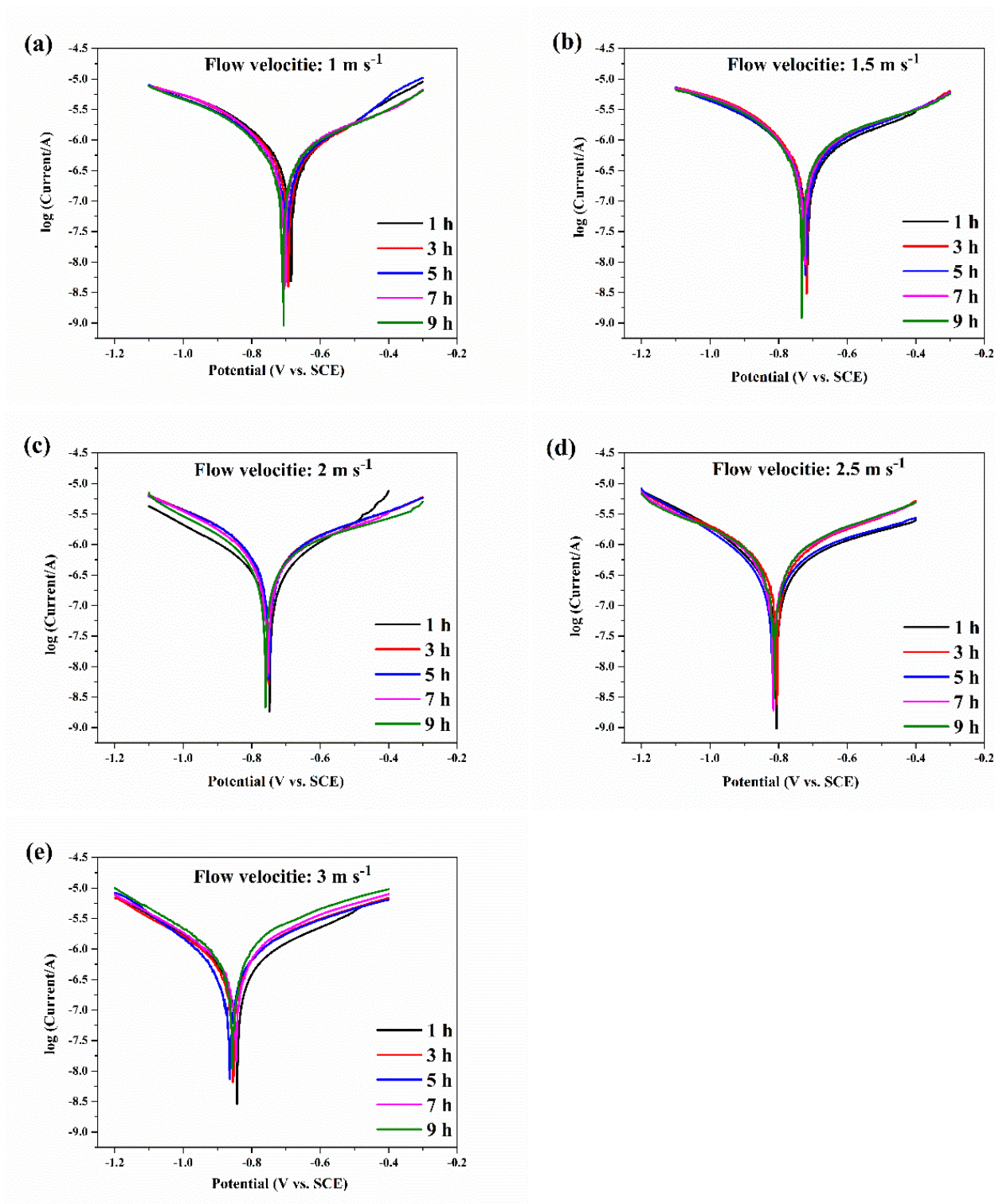
Figure 2. Potentidynamic polarization curves of the aluminum electrodes at various water flow velocities of 1 (a), 1.5 (b), 2 (c), 2.5 (d), and 3 m s⁻¹ (e).

The corrosion potentials and corrosion current densities of aluminum electrodes at various water flow velocities are shown in Table 1. With increasing erosion time, the corrosion currents of the aluminum electrodes under various water flow velocities were relatively stable and hardly changed. The

corrosion currents gradually increased with increasing water flow velocity. Therefore, the corrosion of the aluminum electrodes increased with increasing water flow velocity. The passivation films on the aluminum surfaces were destroyed by erosion. At the moment the protective abilities of the passivation films began to decrease, the corrosion gradually increased. In addition, the diffusion of oxygen in the solution increased with increasing water flow velocity, and the corrosion reaction rate of the aluminum electrodes increased [22].

Table 1. Corrosion potentials, current densities and Tafel slopes of the aluminum electrodes.

Water flow velocities (m s^{-1})	Erosion time (h)	Corrosion potential (V)	Corrosion current density (10^{-7} A cm^{-2})	Anodic Tafel slope (V dec^{-1})	Cathodic Tafel slope (V dec^{-1})
	1	-0.686	3.681	0.231	-0.184
	3	-0.693	3.495	0.239	-0.189
1	5	-0.700	3.575	0.239	-0.185
	7	-0.704	3.472	0.237	-0.183
	9	-0.707	3.603	0.232	-0.186
	1	-0.715	4.553	0.232	-0.184
	3	-0.718	4.587	0.228	-0.181
1.5	5	-0.722	4.436	0.232	-0.188
	7	-0.723	4.579	0.233	-0.188
	9	-0.733	4.664	0.231	-0.187
	1	-0.751	4.946	0.232	-0.185
	3	-0.749	4.910	0.229	-0.181
2	5	-0.748	4.887	0.232	-0.189
	7	-0.754	4.939	0.235	-0.188
	9	-0.760	5.064	0.232	-0.180
	1	-0.805	5.756	0.243	-0.167
	3	-0.806	5.873	0.236	-0.161
2.5	5	-0.810	5.648	0.235	-0.163
	7	-0.814	5.832	0.241	-0.164
	9	-0.816	5.721	0.237	-0.168
	1	-0.843	6.437	0.223	-0.178
	3	-0.855	6.358	0.221	-0.179
3	5	-0.864	6.515	0.224	-0.176
	7	-0.845	6.376	0.223	-0.180
	9	-0.857	6.497	0.222	-0.178

3.2. EIS

The EIS curves of the aluminum electrodes are shown in Fig. 3a-e. The Nyquist diagrams for the electrochemical corrosion of the aluminum electrodes under various water flow velocities were similar, with a semicircle and a straight line. The semicircular diameter in the high frequency region represents the charge transfer impedance (Rct) of the corrosion reaction, which reflects the corrosion resistance of the aluminum in the solution. The equivalent circuit diagram is shown in Fig. 3f. R1 represents the solution resistance between the aluminum electrode and the reference electrode, R2 represents the impedance of the electrolyte through the deposition layer, R3 represents the charge transfer impedance

for the oxidation of aluminum, C1 represents the capacitance of the cladding layer, C2 represents the capacitance of the double layer, and W represents the diffusion impedance of the ions in the electrolyte [23, 24]. The fitted curves were well matched to the experimental data, which indicated that the equivalent circuit diagram was representative of the corrosion reaction of aluminum in the electrolyte.
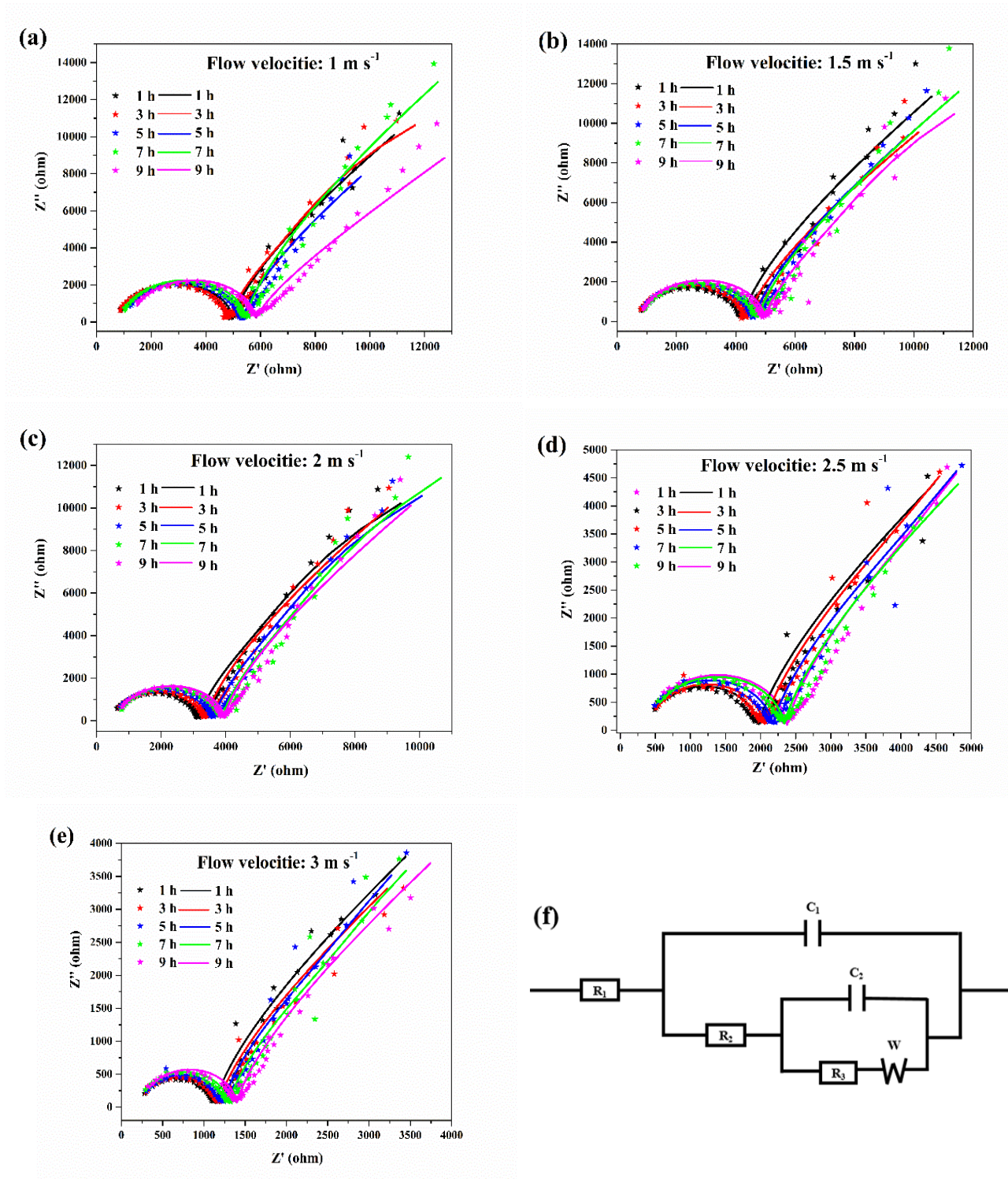

Figure 3. EIS curves of the aluminum electrodes with various water flow velocities, 1 (a), 1.5 (b), 2 (c), 2.5 (d), and 3 m s⁻¹ (e), and their associated equivalent circuit diagram (f). The original data curves and the fitting curves are indicated by a dotted line and a solid line, respectively.

The data for the corresponding numerical simulation of the equivalent circuit diagram are shown in Table 2. The charge transfer resistance of the aluminum electrodes tended to be stable with increasing erosion time. The charge transfer impedance gradually decreased with increasing water flow velocity, and the aluminum corrosion intensified. This result was consistent with the potentidynamic polarization curves.
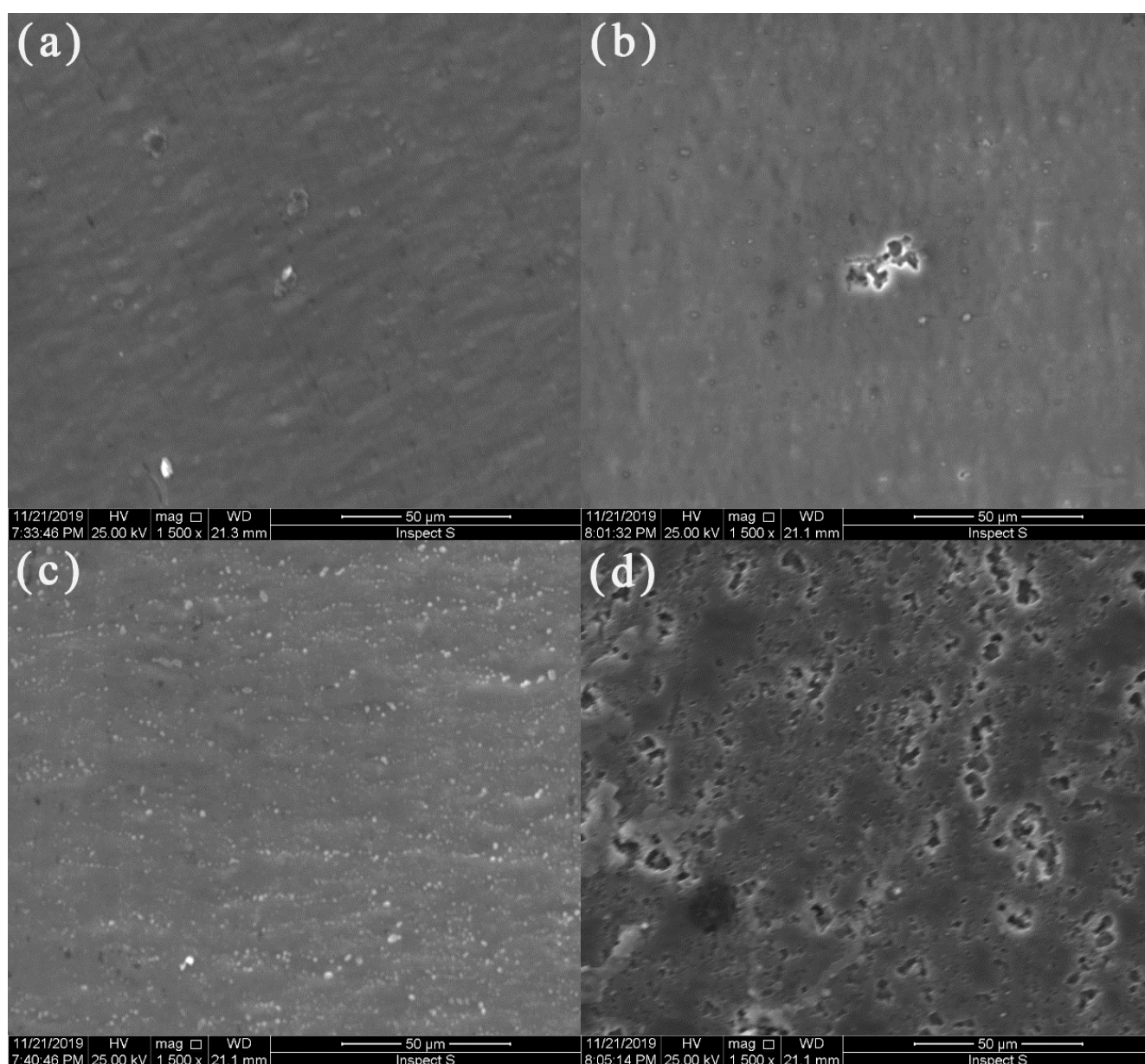
Table 2. EIS parameters of the aluminum electrodes obtained by fitting the data to the equivalent circuit model.

Flow rate $(m\ s^{-1})$	Erosion time (h)	R1 $(10^{-2}\ \Omega)$	R2 $(10^{-3}\ \Omega)$	R3 $(10^{-5}\ \Omega)$	C1 $(10^{-6}\ F)$	C2 $(10^{-6}\ F)$
	1	3.462	3.985	5.348	7.263	5.634
	3	3.294	4.087	5.636	7.132	5.551
1	5	3.567	4.159	5.854	6.523	5.267
	7	3.268	4.472	6.024	7.032	5.589
	9	3.154	4.640	6.326	7.462	5.647
	1	3.884	3.766	4.181	7.798	5.526
	3	3.361	3.727	4.380	6.567	5.301
1.5	5	3.963	3.809	4.536	7.128	5.182
	7	3.336	3.949	4.672	7.728	5.459
	9	3.733	3.836	4.936	7.199	5.498
	1	3.581	2.717	3.602	7.814	7.762
	3	3.754	2.884	3.848	6.932	6.631
2	5	3.885	3.171	3.919	7.125	7.085
	7	3.744	2.951	4.034	7.664	7.011
	9	3.803	3.021	4.111	7.169	7.526
	1	3.405	1462	2.753	7.458	6.887
	3	3.740	2.284	2.924	7.287	6.981
2.5	5	3.857	1.715	2.805	7.027	6.773
	7	3.797	1.564	3.138	6.407	7.440
	9	3.528	2.836	3.216	7.754	6.849
	1	3.364	0.899	1.883	7.009	6.594
	3	3.015	0.990	1.751	7.224	7.513
3	5	3.333	1.068	2.039	7.098	5.605
	7	3.491	1.084	2.171	7.028	6.084
	9	3.424	1.039	2.479	6.642	6.227

The effect of water flow velocity on erosion corrosion was mainly realized by the mass transfer process [25, 26]. When the water flow velocity was low, the passivation film on the aluminum surface could stably form, and the substrate was protected; thus, the corrosion was weak. Forced convection began to appear with increasing water flow velocity, and the passivation film on the aluminum surface was destroyed due to stress. The protective ability of the passivation film decreased, and the aluminum corrosion gradually increased. In addition, the diffusion of oxygen in the solution accelerated with increasing water flow velocities, which accelerated the corrosion reaction.

3.3. SEM

The surface morphologies of the aluminum electrode surfaces after potentiostatic anodic oxidation at 0.5 V for 0.5 h in 50 °C deionized water and under various water flow velocities are shown in Fig. 4. As shown in Fig. 4c, d, obvious corrosion phenomena could be observed when the water flow velocities were at high rates of 2.5 and 3 m s^{-1}. There were gullies and corrosion products on the aluminum electrode surfaces. In contrast, the corrosion of aluminum electrodes with low water flow velocities was relatively mild. As shown in Fig. 4a-c, only a small number of corrosion pits and corrosion product particles appeared on the electrode surface. It was indicated that with increasing water flow velocities, the corrosion pits became larger, the corrosion products were more abundant, and the aluminum surface corrosion became more serious. The above result was consistent with the potentidynamic polarization curves and EIS results.
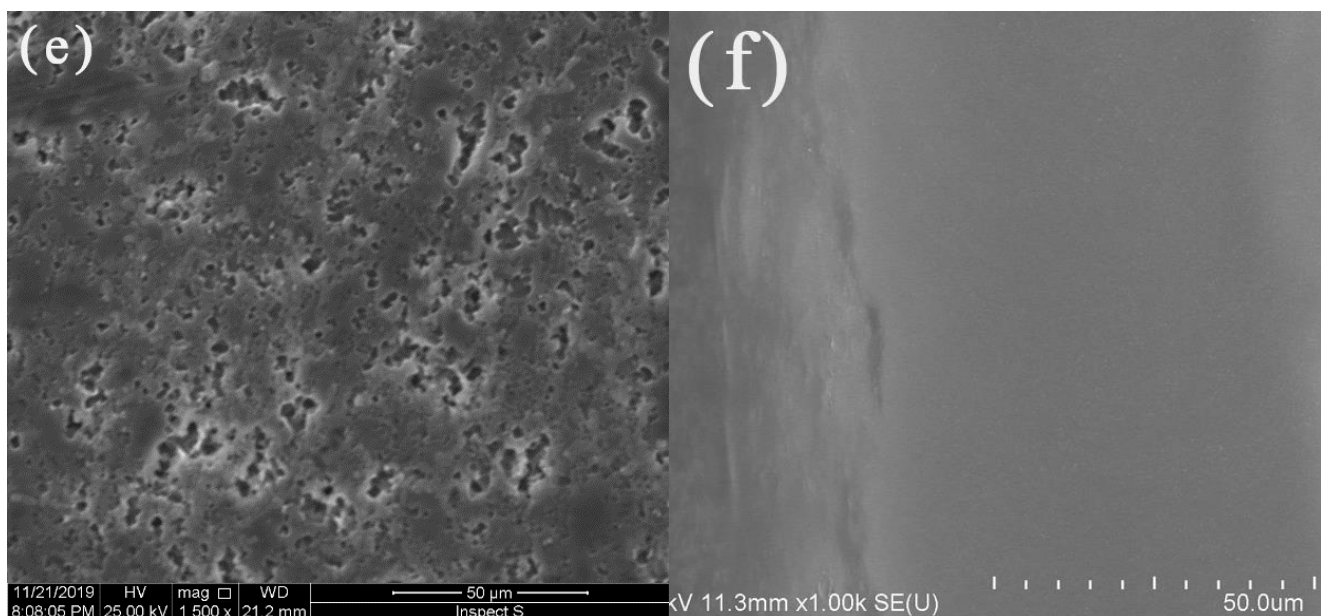
Figure 4. SEM images of the corrosion products for the aluminum electrode surfaces after potentiostatic anodic oxidation at 0.5 V for 0.5 h in 50 °C deionized water under various water flow velocities of 1 m s^{-1} (a), 1.5 m s^{-1} (b), 2 m s^{-1} (c), 2.5 m s^{-1} (d), and 3 m s^{-1} (e). SEM images (f) of the aluminum electrode cross-section after a potentiostatic anodic oxidation under 0.5 V for 0.5 h in 50 °C deionized water under a water flow velocity of 3 m s^{-1}.

SEM images of the aluminum electrode cross-section after potentiostatic anodic oxidation at 0.5 V for 0.5 h in 50 °C deionized water under a water flow velocity of 3 m s^{-1} is shown in Fig. 4f. There were significant differences between the outer corrosion product layer and the aluminum interior, and there were obvious interfaces. The thickness of the corrosion product layer was ~30 μm.
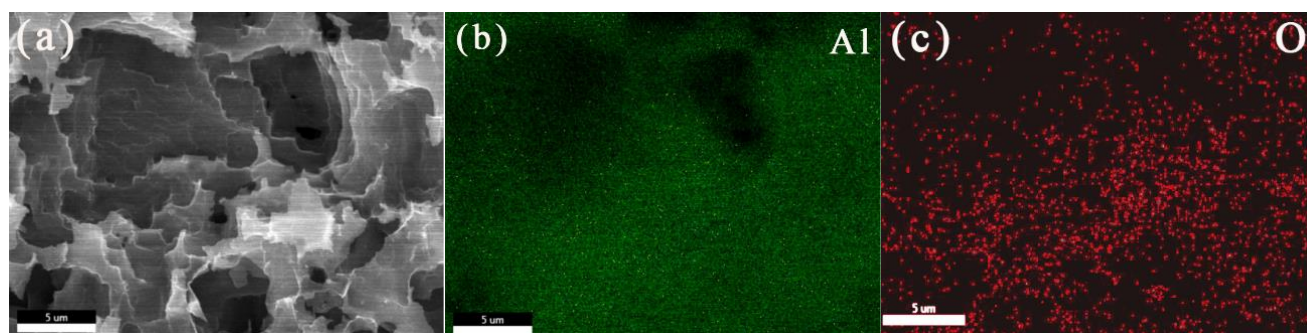
3.4. EDS

Figure 5. SEM image (a) and the EDS elemental analysis of Al (b) and O (c) in the corrosion products on the aluminum electrode surface after potentiostatic anodic oxidation at 0.5 V for 0.5 h in 50 °C deionized water under a water flow velocity of 3 m s^{-1}.

An EDS diagram of the corrosion products on the aluminum electrode after potentiostatic anodic oxidation at 0.5 V for 0.5 h in 50 °C deionized water under a water flow velocity of 3 m s^{-1} is shown in Fig. 5. The elemental compositions of the corrosion products were mainly aluminum and oxygen. The

atomic ratios of aluminum and oxygen were 87.4% and 12.6%, respectively. Aluminum was uniformly distributed on the electrode surface, and oxygen was mainly concentrated in the corrosion products.

3.5. IR

The IR spectrum of the corrosion products on the aluminum electrode surface is shown in Fig. 6a. The sample had a series of strong absorption peaks at 3286, 2967, 2924, and 2862 cm^{-1}, which were caused by the stretching vibration of hydroxyl (-OH). The absorption peaks at 1532 and 1452 cm^{-1} were caused by the deformation vibration of hydroxyl (-OH). The stretching vibrations of the absorption peaks at 1067, 1003 and 910 cm^{-1} corresponded to the Al-O bond [27, 28]. The IR results confirmed that the corrosion products were mainly $Al(OH)_3$.
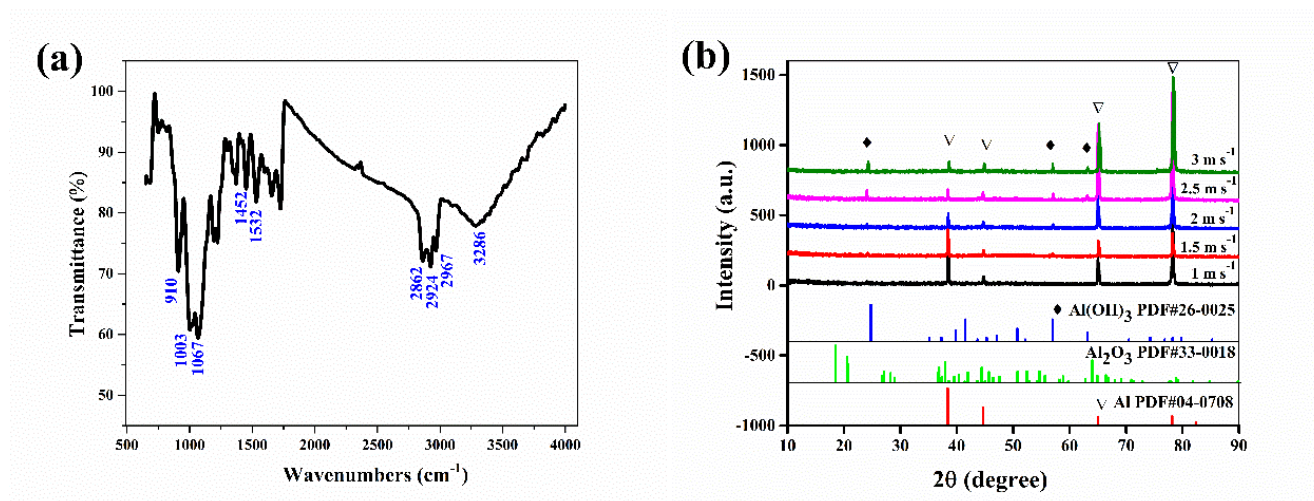

Figure 6. IR spectrum (a) of the aluminum electrode surface after potentiostatic anodic oxidation at 0.5 V for 0.5 h in 50 °C deionized water under a water flow velocity of 3 m s^{-1}, and XRD spectra (b) of the aluminum electrodes under various water flow velocities.

3.6. XRD

XRD spectra of the aluminum electrode surface after potentiostatic anodic oxidation at 0.5 V for 0.5 h in 50 °C deionized water under various water flow velocities is shown in Fig. 6b. For all the samples, there were four strong peaks at 39°, 45°, 65° and 78°. These peaks matched well to Al (PDF#040-708). The peaks at 25°, 57° and 63° could also correspond to the peaks of the standard card of $Al(OH)_3$ (PDF # 26-0025), so the corrosion products were mainly $Al(OH)_3$. The aluminum corrosion in deionized water accelerated under constant potential anodic oxidation. The hydrogen evolution reaction at the cathode made the solution alkaline, and the anodic dissolution reaction and corrosion reaction occurred at the anode. The corrosion products in the alkaline environment were basically $Al(OH)_3$. With increasing water flow velocity, the peaks of $Al(OH)_3$ in the corrosion products at 25°,

57° and 63° gradually increased. The corrosion products on the aluminum surface gradually increased, and the aluminum corrosion gradually became serious.

4. CONCLUSIONS

With increasing water flow velocities, the corrosion current of aluminum electrodes gradually increased, the charge transfer resistance gradually decreased, and the corrosion became more serious. When the water flow velocities were low, the passivation film on the aluminum surface could be stably formed and could protect the substrate. Forced convection occurred with increasing water flow velocities. The stress on the aluminum surface destroyed the passivation film, and the corrosion gradually increased. Considering the actual situation in which aluminum has been subjected to erosion corrosion in an HVDC inner water cooling system, the erosion corrosion characteristics of aluminum were studied. The results will be helpful for optimization the technology and parameters of an HVDC thyristor valve cooling system.

References

1. A. Kalair, N. Abas, N. Khan, *Renew. Sust. Energ. Rev.*, 59 (2016) 1653.
2. B.V. Eeckhout, D.V. Hertem, M. Reza, K. Srivastava, R. Belmans, *Eur. T. Electr. Power*, 20 (2010) 661.
3. C. Wang, X. Liu, X. Wang, N. Liu, X. Jiao, Y. Tan, *IEEE Electr. Insul. Conf.*, Washington, 2015, 24.
4. P.O. Jackson, B. Abrahamsson, D. Gustavsson, L. Igetoft, *IEEE T. Power Deliver.*, 12 (1997) 1049.
5. H.P. Lips, *IEEE T. Power Deliver.*, 9 (1994) 1830.
6. I. Weber, B. Mallick, M. Schild, S. Kareth, R. Puchta, R. Eldik, *Chem. Eur. J.*, 20 (2014) 12091.
7. B. Gao, T. He, F, Yang, C. Liu, X. Song, Y. Cheng, *IEEE Access*, 7 (2019) 67960.
8. D. Li, Y. Shi, H. Xu, Y. Chen, P. Zhou, X. Li, W. Feng and S. Wang, *Int. J. Electrochem. Sci.*, 13 (2018) 9346.
9. D. Li, Z. Shi, H. Xu, Y. Chen, W. Feng, Z. Qiu, H. Liu, G. Lv, S. Wang, Y. Fan, *Int. J. Electrochem. Sci.*, 14 (2019) 3465.
10. F. Zheng, L. Hao, J. Li, H. Zhu, X. Chen, Z. Shi, S. Wang, Y. Fan, *Int. J. Electrochem. Sci.*, 14 (2019) 7303.
11. J.G. Chacon Nava, F.H. Stott, M.M. Stack, *Corros. Sci.*, 35 (1993)1045.
12. Y. Zheng, Z. Yao, X. Wei, W. Ke, *Wear*, 186-187 (1995) 555.
13. D.C. Wen, *J. Mater. Sci.*, 44 (2009) 6363.
14. G.A. Zhang, L.Y. Xu, Y.F. Cheng, *Corros. Sci.*, 51 (2009) 283.
15. S.W. Watson, F.J. Friedersdorf, B.W. Madsen, S.D. Cramer, *Wear*, 181-183 (1995) 476.
16. E. Deltombe, M. Pourbaix, *Corrosion*, 14 (1958) 16.
17. M.V. Prozhega, N.A. Tatus, S.V. Samsonov, O.Yu. KolyuzhniE, N.N. Smirnov, *J. Frict. Wear*, 35 (2014) 155.
18. M.M. Stack, N. Corlett, S. Turgoose, *Wear*, 255 (2003) 225.
19. C.Y. Kong, R.C. Soar, P.M. Dickens, *J. Mater. Process Tech.*, 146 (2004) 181.
20. T.S. Huang, G.S. Frankel, *Corros. Sci.*, 49 (2007) 858.

21. E.M. Sherif, S.M. Park, *Electrochim. Acta*, 51 (2006) 1313.
22. L. Niu, Y.F. Cheng, *Wear*, 265 (2008) 367.
23. P.J. Eng, T.P. Trainor, G.E. Brown Jr., G.A. Waychunas, M. Newville, S.R. Srtton, M.L. Rivers, *Science*, 288 (2000) 1029.
24. E.J. Lee, S.I. Pyun, *Corros. Sci.*, 37 (1995) 157.
25. J. Zhang, M. Klasky, and B.C. Letellier, *J. Nucl. Mater.*, 384 (2009) 175.
26. T.Y. Chen, A.A. Moccari, D.D. Macdonald, *Corrosion*, 48 (1992) 239.
27. N. Phambu, *Mater. Lett.*, 57 (2003) 2907.
28. W. Zhang, P. Li, H.B. Xu, R. Sun, P. Qing, Y. Zhang, *J. Hazard. Mater.*, 268 (2014) 273.